Journal of Structural Geology, Vol. 15, No. 6, pp. 721 to 735, 1993
Printed in Great Britain

0191-8141/93 $06.00+0.00

Displacement and deformation associated with a lateral thrust termination, southern Golden Gate Range, southern Nevada, U.S.A.

PHILLIP A. ARMSTRONG and JOHN M. BARTLEY

Department of Geology and Geophysics, University of Utah, Salt Lake City, UT 84112, U.S.A.

(*Received* 23 *April* 1991; *accepted in revised form* 13 *August* 1992)

Abstract—The Golden Gate thrust offers an excellent opportunity to study displacement and deformation at a lateral thrust tip. Slip across this E-vergent thrust is uniformly about 2.4 km for the southern 2 km of exposed strike length and dies out to zero in the northern 5 km. Constant displacement and uniform hangingwall structure along the southern one-third of exposed strike length suggest that along-strike displacement variation and consequent deformation are localized near the lateral tip.

Structures located at and north of the lateral tip are consistent with transpression and later uplift as slip accumulated on the thrust. Fold and fault orientations and calcite twinning strain record possible transpression north of the lateral tip. E–W-striking normal faults at the thrust tip record extension that is interpreted to be the result of the uplift and translation of a structurally continuous, rigid block located north of the normal faults. This block is connected to and was uplifted with the crest of the hangingwall anticline, and was separated by the normal faults from thrust-related folding to the south.

The main hangingwall structure is an anticline that in southern exposures trends N–S parallel to the thrust but bends westward and opens into a box fold to the north. The hangingwall anticline superficially resembles a classic fault-propagation fold formed by a migrating ductile bead. However, we are forced to reject the ductile bead hypothesis for the fold because: (1) the geometry of the hangingwall anticline far from the thrust tip cannot have evolved from the geometry at the thrust tip; and (2) twinned calcite strain data from along the thrust suggest that strain was homogeneous and coaxial rather than inhomogeneous and progressively non-coaxial as predicted for a migrating ductile bead. The three-dimensional structural and kinematic relations at the lateral tip of the Golden Gate thrust appear to be the result of deformation around a pinned tip, although the reason that the tip was pinned at its present location is unclear. We interpret the thrust to have propagated relatively quickly to its ultimate extent with little initial displacement, indicating that it was easier to fault the rocks than to fold them.

INTRODUCTION

FAULT slip is zero at a fault termination and, in the ideal case of a crack in a homogeneous elastic material, increases monotonically toward the center of the slipped fault patch. Crack slip and propagation cause large secondary stresses near crack terminations (Hertzberg 1976). For elastic–plastic materials such as upper crustal rocks, volumes in which secondary stresses near a fault termination are large relative to regional stress magnitudes undergo strain patterns that differ from those away from the termination. In this study we address the changes in displacement and in deformation patterns resulting from changes in the induced stress field along strike of a thrust fault and in the vicinity of its exposed lateral termination.

Since at least 1921 it has been known that ramping thrusts, unless they transfer their slip to other faults, die out laterally into asymmetric folds (Heim 1921). Elliott (1976) suggested that these folds formed along the frontal and lateral tip line by progressive thrust propagation and termed this deformation front the ductile bead. In the ductile bead model, the thrust propagates in the frontal direction, parallel to the slip direction, and laterally, perpendicular to the slip direction. These propagation processes are kinematically equivalent to edge dislocations (frontal) and screw dislocations (lateral) in crystal lattices. Williams & Chapman (1983) called the strain imparted during formation of the ductile bead 'background' strain and suggested that subsequent deformation is taken up as slip along the fault plane. In other words, the fold at the ductile bead may not be modified after propagation of the thrust through it, but may ride passively in the hangingwall. Geometric models of folds that form in the ductile bead (fault-propagation folds; Suppe 1985) suggest that a volume of rock in the propagation zone will be strained differently at different times in its deformation history due to fold-hinge migration. Thus a very complex progressive strain history should be recorded at any one point. Also, the ductile bead process implies that younger 'immature' structures preserved at the lateral tip would, with continued displacement, grow into more 'mature' structures preserved toward the central part of the thrust, i.e. serial cross-sections from the tip toward the center should provide a time-sequential record of ductile bead strain. This set of predictions we refer to as the ductile bead model.

More recently, field evidence has accumulated that suggests that thrust-related structures record effects of fault arrest rather than propagation. In these cases, the fault becomes pinned at its ultimate extent when only small displacement has occurred; structures near the tip then grow as differential displacement accumulates along the fault (Julian & Wiltschko 1983, Fischer & Woodward 1989, 1992). This suggests that, at least in some cases, a fault propagates relatively quickly with little slip until it reaches a location where further expansion of the fault surface is impeded. The propagation stage is followed by accumulation of slip and associated

deformation. This scenario dictates that faulting precedes folding, and it contrasts with the ductile bead scenario in which the fault propagates with and below the fold, causing folding before faulting. The location of the locked tip may be localized by facies and competency changes (Julian & Wiltschko 1983, Fischer & Woodward 1989, 1992).

Abundant information exists on the displacement and deformation associated with *frontal* thrust terminations in which the deformation and faulting is considered in vertical cross-sections drawn parallel to the slip direction (Boyer & Elliott 1982, Williams & Chapman 1983, Chapman & Williams 1984, Jamison 1987, Chester & Chester 1990, Hyett 1990). However, few models and scarce field documentation exist concerning the deformation and displacement associated with *lateral* thrust terminations in which deformation and displacement is considered along strike toward and around exposed thrust tips. This is probably because lateral thrust tips rarely are sufficiently well exposed, thus making confident along-strike displacement and strain measurements difficult. Generally, only the stratigraphic separation (e.g. Evans & Spang 1984) is known from which the actual displacement can only be inferred. Documenting changes in along-strike displacement and principal strain orientations of a well-exposed and constrained thrust fault should help in understanding the deformation processes at lateral tips.

The Golden Gate thrust, located in the southern Golden Gate Range in southern Nevada (Fig. 1) and described in general by Tschanz & Pampeyan (1970), offers an exceptional opportunity to study a lateral thrust termination. The thrust crops out nearly continuously for about 6.5 km, has a well-located lateral termination and well-constrained structural geometry, and offsets a well-characterized stratigraphy which permits accurate displacement measurements along strike. Also, the southern Golden Gate Range behaved essentially as a rigid block during later deformational events, thus allowing direct displacement and strain measurements that do not contain post-thrust reconstruction errors.

In this study we investigate the displacement and deformation relations at and near the lateral tip of the Golden Gate thrust. These relationships were determined using detailed surface mapping and a series of balanced cross-sections across the thrust. Principal strain orientations determined from calcite twinning further document the deformation around the lateral thrust tip.

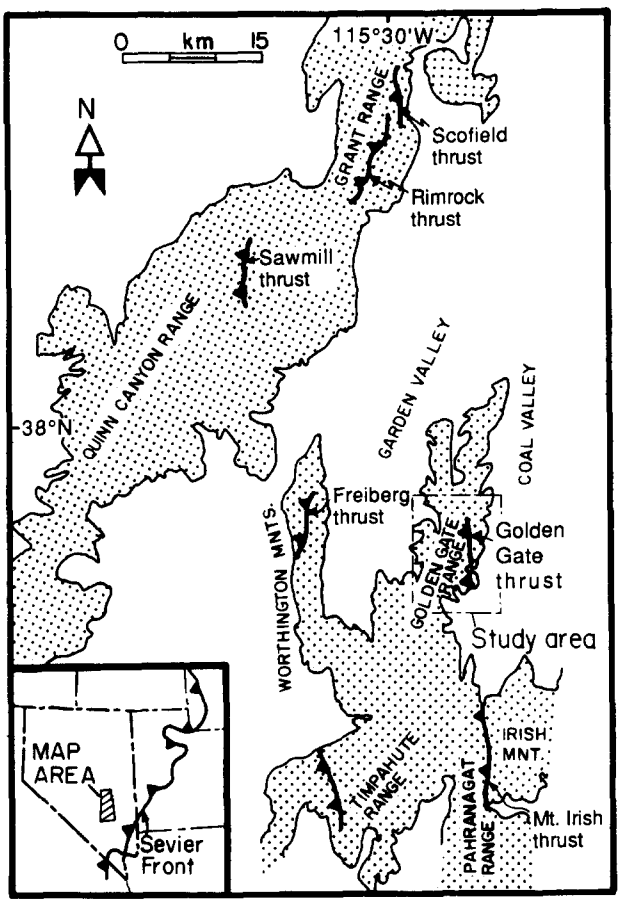

Fig. 1. Location map of the Golden Gate thrust relative to other structures in the Garden Valley area and relative to the Sevier Front. Faults of the Garden Valley thrust system include the Scofield, Rimrock, Sawmill, Freiberg and Golden Gate thrusts.

GEOLOGIC SETTING AND STRATIGRAPHY

The Golden Gate thrust and related folding and faulting reflect E-vergent Mesozoic contraction during the Sevier Orogeny. The thrust is part of a larger system, informally called the Garden Valley thrust system, which comprises at least five exposed thrust faults (Fig. 1). The Garden Valley thrust system is located about 125 km west of the easternmost exposure of the Sevier thrust belt at this latitude (Fig. 1), within the Sevier hinterland of Armstrong (1968). Sevier thrusting probably began in Early Cretaceous (Armstrong 1968, Heller & Paola 1989) and its cessation in this part of Nevada is best, although poorly, constrained by the sub-Oligocene unconformity.

Deformation associated with Tertiary Basin and Range extension is minimal within the southern Golden Gate Range. The consistent stratal orientation (001°/24° W) of Tertiary volcanic rocks on the west side of the range (Fig. 2) and a lack of faulting affecting the sub-Tertiary unconformity suggest that the entire southern Golden Gate Range block was tilted 24°W about a N–S axis due to movement of an E-dipping normal fault located in Garden Valley to the west (Snyder 1983).

Exposed Paleozoic rocks in the southern Golden Gate Range consist of 2200 m of Upper Ordovician through Mississippian miogeoclinal strata (Fig. 3). Limestone and dolomite comprise about 95% of the strata; quartzite and shale are locally interstratified. Carbonate units locally contain abundant invertebrate fossils. This comparatively massive and uniformly calcareous sequence exerted significant control on the character of the structures formed.

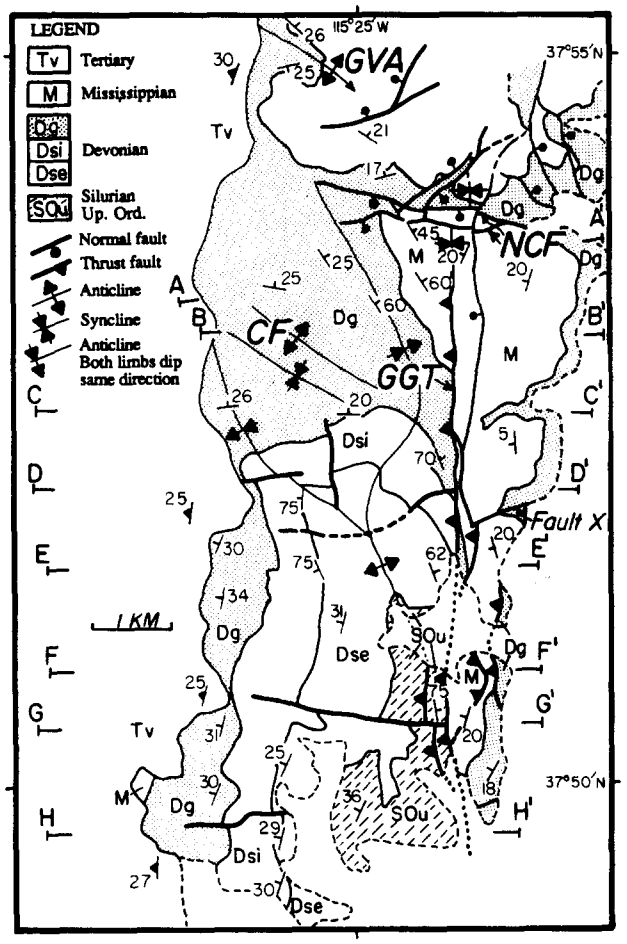

Fig. 2. Generalized geologic map of the southern Golden Gate Range. CF—central folds, GGT—Golden Gate thrust, GVA—Garden Valley anticline and NCF—North Canyon faults. See Fig. 3 for formation names.

THRUST-RELATED STRUCTURES

Golden Gate thrust

The Golden Gate thrust is exposed almost continuously for 6.5 km and is the dominant structural element in the southern Golden Gate Range. It strikes N–S and dips 65–80°W; with Tertiary tilting removed, it has a relatively steep ramp dip of 41–56°W. In the southernmost exposures, the thrust places Ordovician Ely Springs Dolomite on Mississippian Joana Limestone with a maximum stratigraphic separation of 2100 m. The Golden Gate thrust dies out laterally to the north into a syncline (hereafter called a thrust termination syncline) cored by Mississippian Chainman Shale (Fig. 2). Small-scale folds and sparse fault-plane and flexural-slip slickenlines in the footwall indicate an overall transport azimuth of 080–090°.

The Mount Irish thrust, located south of the Golden Gate Range (Fig. 1), has similar hangingwall and footwall stratigraphic relations as the Golden Gate thrust, namely Middle and Upper Ordovician strata thrust over Upper Devonian strata (Tschanz & Pampeyan 1970). Thus, the Golden Gate thrust appears to be the northward continuation of Mount Irish thrust.

Golden Gate thrust splays and imbricates

The Golden Gate thrust separates into two or more splays from south to north (Figs. 2 and 4, sections D–D′ and E–E′). North of section F–F′ the eastern splay bends to the east and then back to the west, where it joins with the western trace and continues north (Fig. 2). The rocks between the splays are nearly vertical and highly attenuated, characteristic of the rocks that dip into the thrust farther north and typical of hangingwall anticline forelimbs in general (Jamison 1987). The vertical rocks are faulted against footwall rocks that dip less than 20°W, relations that match those of the hangingwall and footwall both to the north and south of the splay.

At least two footwall imbricates are located in the vicinity of section F–F′ (Figs. 2 and 4). The imbricate faults parallel their respective hangingwall beds but cut up-section in their footwalls (footwall beds dip about 20° less than the imbricates). This hangingwall flat–footwall ramp geometry directly east of the main trace of the Golden Gate thrust creates space problems between the imbricates and the Golden Gate thrust if the imbricates formed after the main trace. Thus, the imbricates probably formed first.

Other faults related to the Golden Gate thrust

Fault X is a high-angle up-to-the-north fault that strikes N75°E (Fig. 2). It offsets the eastern splay of the Golden Gate thrust, but is cut by the main (western) trace of the thrust and does not continue into the hangingwall (Fig. 2). North and south of fault X, the eastern splay cuts different sections of the Mississippian rocks. These observations suggest that fault X was active during movement on the Golden Gate thrust.

The Golden Gate thrust dies out just south of a set of E–W-striking normal faults that dip 60–80°S (Fig. 2). Collectively, these faults are informally called the North Canyon faults. North of the North Canyon faults, Mississippian and Devonian strata are relatively flat lying, whereas south of the North Canyon faults the same strata dip about 45° or more to the east as part of the eastern limb of the hangingwall anticline (Fig. 2). The cumulative stratigraphic separation across the North Canyon faults decreases to the west from a maximum where the core of the thrust-termination syncline intersects the faults (Fig. 5). Separation goes to zero near the eastern hinge of the hangingwall anticline, where bedding dips change from near horizontal on top of the anticline to E-dipping on the eastern limb (Fig. 2). The 'scissoring' separation of strata on either side of the North Canyon fault zone causes the stratigraphic separation to mimic the fold form of the thrust-termination syncline to the south. The offset of the thrust-termination syncline (projected into an E–W vertical plane) across the North Canyon fault system has a 370 m dextral component and a 730 m dip-slip component (Fig. 5). These observations indicate that the North Canyon fault system formed during folding and at least partly accommodated distortion around the thrust tip.

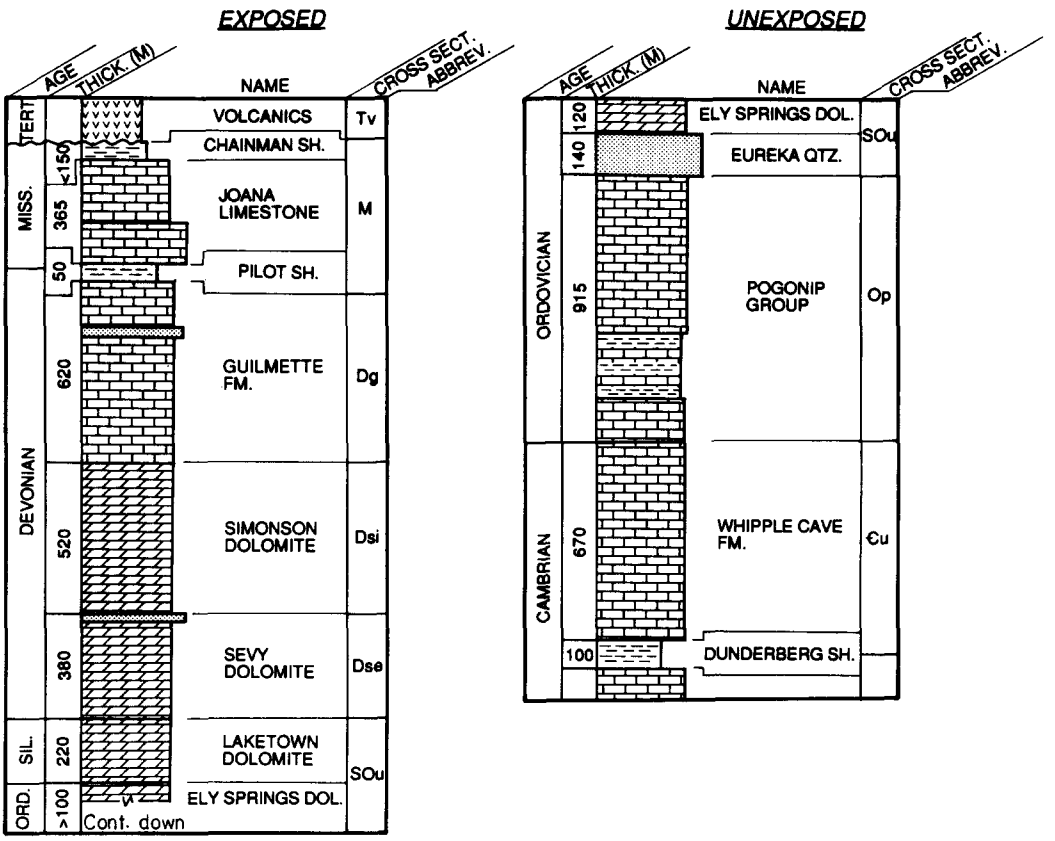

Fig. 3. Generalized stratigraphic column for exposed and unexposed rocks in the southern Golden Gate Range. This section corresponds well with sections exposed farther south described by Reso (1963). Unexposed stratal thicknesses from Reso (1963).

A set of NE-striking normal faults are located north of the North Canyon faults (Fig. 2). Some of these faults cut and are cut by faults of the North Canyon fault system, indicating they are about the same age as both the North Canyon faults and folding at the thrust termination.

Bedding orientations and folds

Bedding orientations in the southern Golden Gate Range fall into three regions according to location with respect to the Golden Gate thrust and North Canyon faults (Fig. 6). Region I includes strongly folded rocks in the hangingwall of the thrust, Region II includes weakly folded rocks north of the North Canyon faults, and Region III includes the largely unfolded rocks in the footwall of the thrust.

The most prominent feature in Region I is a hangingwall anticline informally named the Golden Gate anticline. The oldest exposed rocks of the study area crop out in the southernmost part of the Golden Gate anticline and lie adjacent to the segment of the thrust that has the greatest displacement. The exposed western limb consistently dips 25–30°W across nearly the entire southern part of the field area west of the thrust (Fig. 4, sections F–F′, G–G′ and H–H′ and Fig. 6).

Farther north, the hinge-surface trace of the Golden Gate anticline (Figs. 2 and 4, sections D–D′ and E–E′) bifurcates into hinges that separate a flat top from the eastern and western steep limbs of a large box fold. The hinges dividing the flat and steep limbs plunge gently with moderately inclined hinge surfaces. The northern Golden Gate anticline as a whole trends 342° and plunges 16°. The steep backlimb shallows to dips of about 30°W just east of the Tertiary unconformity (Fig. 4, sections D–D′ and E–E′). Still farther north, the flat-top rocks and the western hinge also project westward under Tertiary cover. Within the flat top of the box fold, a broad, open anticline–syncline pair, informally named the central folds (CF in Figs. 2, 4 and 6) trend 317°, i.e. 25° counterclockwise relative to the northern Golden Gate anticline.

Stratigraphic units within the eastern steep limb of the Golden Gate anticline are thinned an average of about 20% relative to the same units in the rest of the field area. However, thinning varies from 0 to 40% from one unit to another. Differential thinning of formations presents strain compatibility problems that cannot be resolved with current data. The heterogeneity may, however, result from changes in amounts of extension accommodated locally by flexural-slip between units parallel to the forelimb. The thinning of the Golden Gate anticline forelimb is consistent with the forelimb thinning curves of Jamison (1987) given ramp and interlimb angles of 40–60° and 80–100°, respectively.

The most prominent fold in Region II is an open anticline informally named the Garden Valley anticline (Fig. 6). The Garden Valley anticline plunges 6° with a trend of 129°, i.e. subparallel to the central folds (Fig. 6). The similar geometry, orientation and position relative

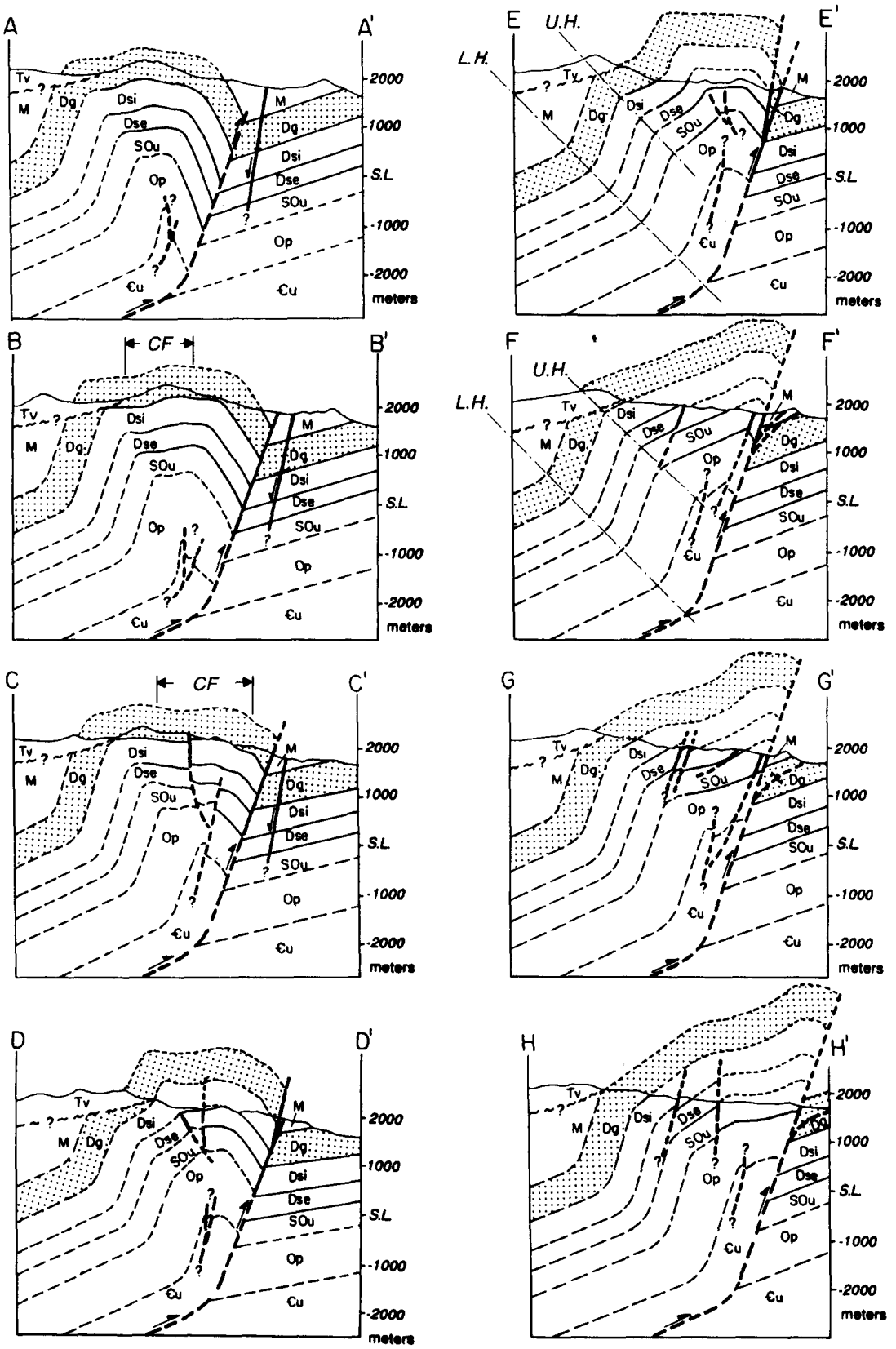

Fig. 4. Generalized cross-sections across the Golden Gate thrust. All Tertiary deformation except 24° Tertiary tilt has been removed. Rock units labels as in Fig. 3. CF—central folds, U.H.—upper hinge and L.H.—lower hinge (see text).

to the Golden Gate thrust of the Garden Valley anticline and central folds suggests a similar kinematic origin for these folds.

With the exception of sparse meter-scale E-vergent kink folds, Region III is unfolded. The eastern limb of the thrust-termination syncline dips about 20°W. South of the syncline, bedding data divide into two subregions that are separated by fault X (Fig. 2). South of fault X beds generally dip about 30°W, whereas north of fault X bedding orientations average near horizontal (Fig. 6).

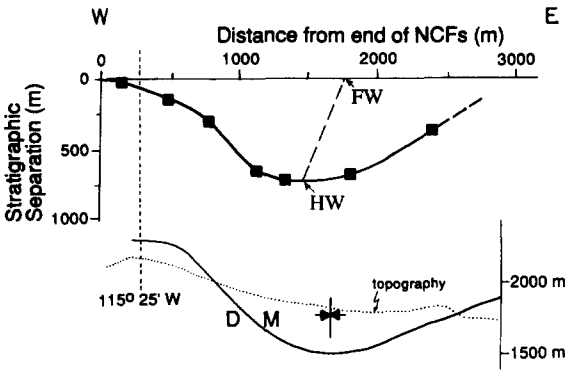

Fig. 5. Cumulative separation of Mississippian(M)–Devonian(D) contact across North Canyon faults vs distance from their western termination, compared to the synclinal fold form from cross section A–A'. On the graph, the dashed line connects the axis of the thrust-termination syncline in the footwall to that in the hangingwall and shows the cumulative offset of the syncline, projected into the E–W vertical plane, across the North Canyon fault system. The position of 115° 25'W longitude is used as a datum for relative locations of the diagrams. FW—footwall, HW—hanging wall.

The change in bedding orientation across fault X is similar to the dip change across the North Canyon faults east of the Golden Gate thrust projection.

GOLDEN GATE THRUST DISPLACEMENT

Eight cross-sections were constructed to evaluate along-strike displacement variations across the Golden Gate thrust (Fig. 4). The cross-sections were balanced locally according to rules presented by many previous authors (e.g. Dahlstrom 1969, Suppe 1983, Woodward *et al.* 1985, De Paor 1988, Geiser 1988) and may not reflect structural complexities that arise from unknown layer-parallel shear, duplexing, or faulting concealed at depth. Additional assumptions for construction of unexposed or upward-projected relations include the following. (1) Rock units, except in the forelimb of the Golden Gate anticline and in thickened hinge zones, are of constant thickness. The queried faults in the core of the Golden Gate anticline are required to balance the section. Although these are schematic, minor reverse faults

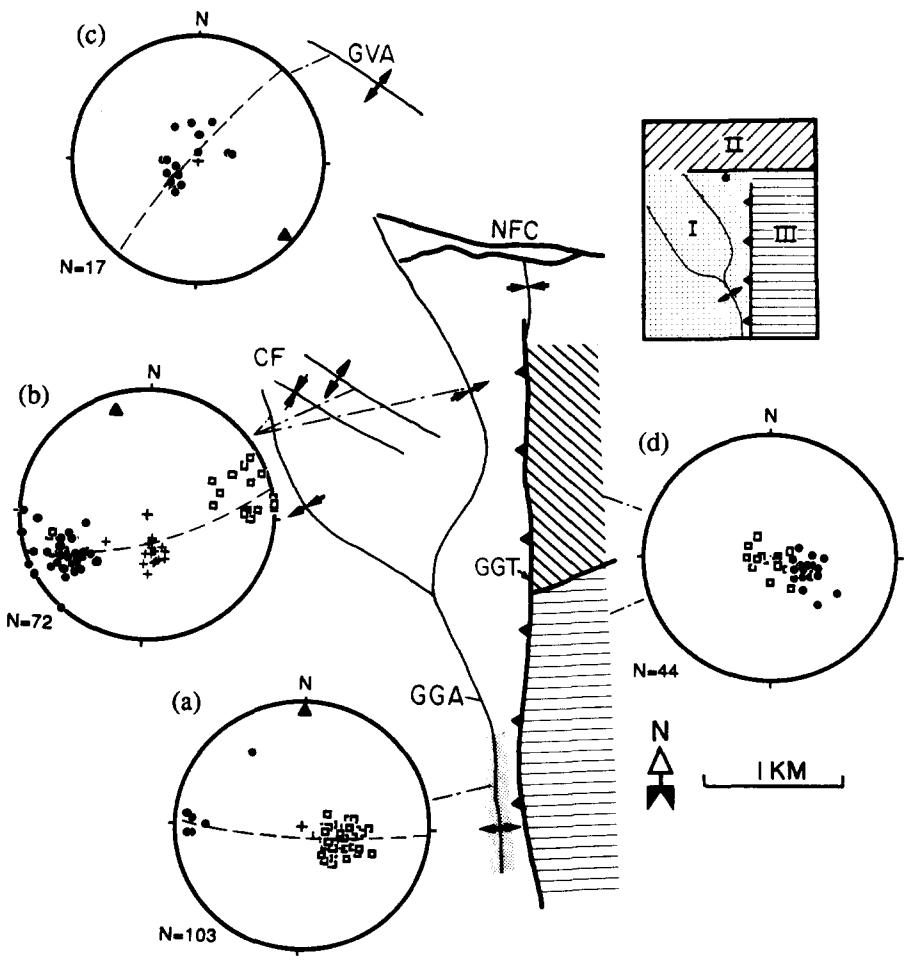

Fig. 6. Map showing locations and equal-area stereoplots of poles to bedding. Dashed great circles are best-fit great circles through the poles picked by the Bingham axial distribution analysis using *Stereonet* by R. W. Allmendinger. Filled triangles represent best-fit fold axis orientations. Other symbols used in specific regions: (a) eastern limb (dots) and western limb (squares) of the southern Golden Gate anticline; (b) eastern steep limb (dots), flat top (pluses), and western steep limb (squares) of the northern Golden Gate anticline. (d) North of fault X in Fig. 2 (squares) and south of fault X (dots). Inset shows bedding orientation regions as discussed in text. CF—central folds, GVA—Garden Valley anticline, GGA—Golden Gate anticline and NCF—North Canyon faults.

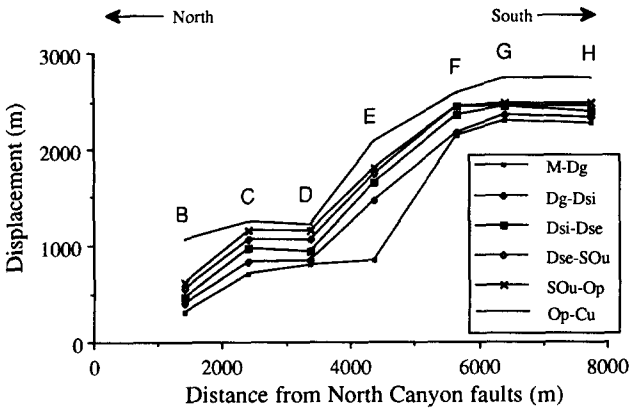

Fig. 7. Displacement vs distance along strike for six contacts. See Fig. 3 for unit abbreviations. Letters refer to cross-sections, e.g. E refers to cross-section E–E′.

commonly crop out within the anticline. (2) Forelimb rock units where projected are thinned by 20%, consistent with exposed forelimb units. (3) Surface bedding dips project to depth and into the air. (4) The Golden Gate thrust loses displacement toward the frontal tip. Unless slip is transferred to other faults, thrust displacement must decrease toward the frontal tip where differential displacement is generally accommodated by folding (Dahlstrom 1969, Chapman & Williams 1984, 1985, Rowan & Ratliff 1988). In practice, this assumption only affects the range of uncertainties (see Appendix) for displacement measurements. (5) No substantial layer-parallel shear (except small amounts recorded by calcite twinning discussed later) occurred in the footwall east of the Golden Gate thrust nor in the hangingwall flat in the Garden Valley region. (6) The main segment of the Golden Gate thrust presently dips 70°W, is planar, and flattens at depth into a W-dipping, bedding-parallel detachment in the Middle Cambrian Dunderberg Shale (Fig. 3). Where the thrust crops out, it presently dips at a high angle with Upper Ordovician rocks in the hangingwall, indicating that the base of the ramp is no shallower than Upper Ordovician strata in the footwall. Geometric arguments related to the location of the upper and lower backlimb hinges (Suppe 1985) indicate that the actual detachment depth probably is deeper. The location of the ramp–flat intersection is determined by the intersection of the thrust ramp and the lower hinge (L.H. on Fig. 4). The upper hinge (U.H. on Fig. 4) is assumed to be everywhere buried under volcanic rocks to the west. With the upper hinge located as far east as possible and assuming that the footwall contacts must project into hangingwall flat contacts, the minimum detachment depth coincides with the anticipated depth of the Cambrian Dunderberg Shale. Moving the upper hinge farther west requires the detachment depth to be deeper but does not affect the interpretations of this study.

Contact separations (Fig. 7) were measured directly from the cross sections and are subject to the construction assumptions. Separations are interpreted as displacements because the cross sections are parallel to the transport direction. In this analysis, a lateral displacement gradient is the dimensionless ratio of the change of dip-slip displacement to distance along the thrust strike. Displacement uncertainties and the criteria for estimating them are given in the Appendix.

Displacement is consistently about 2.4 km for the best constrained contacts in the southern three cross-sections (sections F–F′, G–G′ and H–H′ in Fig. 4), and the lateral displacement gradient is near zero (Fig. 7). North of section F–F′ the displacement decreases northward. Between sections F–F′ and D–D′ the lateral displacement gradient is about 0.48 for the best constrained contacts. Between sections D–D′ and C–C′ the gradient decreases to near zero because of the relatively low displacements of all contacts in section D–D′ which crosses the near-horizontal footwall rocks just north of fault X (Fig. 2). Between sections C–C′ and B–B′ the gradient again increases to about 0.36. If cross-section D–D′ were neglected, the lateral displacement gradient would be nearly constant and about 0.42 between sections B–B′ and F–F′. These observations indicate that all of the displacement variation occurs within about 5 km of the exposed lateral tip of the thrust, coincident with most of the hangingwall folding, the counterclockwise bend of the Golden Gate anticline, and splaying of the Golden Gate thrust (Fig. 2).

The correlative Mount Irish thrust about 15 km south juxtaposes the same units, in a similar geometry, as the southern part of the Golden Gate thrust. Combined with constant displacement and structural similarity of the hangingwall rocks along one-third of the exposed fault length in the southern Golden Gate Range (sections F–F′, G–G′ and H–H′, in Fig. 4), this suggests that there is little variation in along-strike displacement or hangingwall internal deformation. Thus, nearly all the lateral variation in displacement and hangingwall deformation is localized near the lateral tip of the Golden Gate thrust.

CALCITE STRAIN ANALYSIS

The calcite strain-gage technique of Groshong (1972) was used to determine variations in principal strain orientations along the Golden Gate thrust and around its lateral tip. The details of the calcite strain-gage technique are discussed by Groshong (1972, 1974), Spang & Van Der Lee (1975), Teufel (1980) and Groshong *et al.* (1984).

Fourteen samples were analyzed from locations shown in Fig. 8. Two or three mutually perpendicular thin sections were cut from each sample and, following Groshong *et al.* (1984), at least 25 twin sets were measured from each of two sections. All of the twin sets observed in a grain were measured; twins that extended partially across the grain were treated as whole twins. Twins were measured in both sparry material and fossil grains (Table 1), but calcite-filled veins were avoided. Outcrop descriptions of the samples are given in Table 2.

In most samples 80–90% of the twins measured were microtwins. The amount of twinned material in a micro-

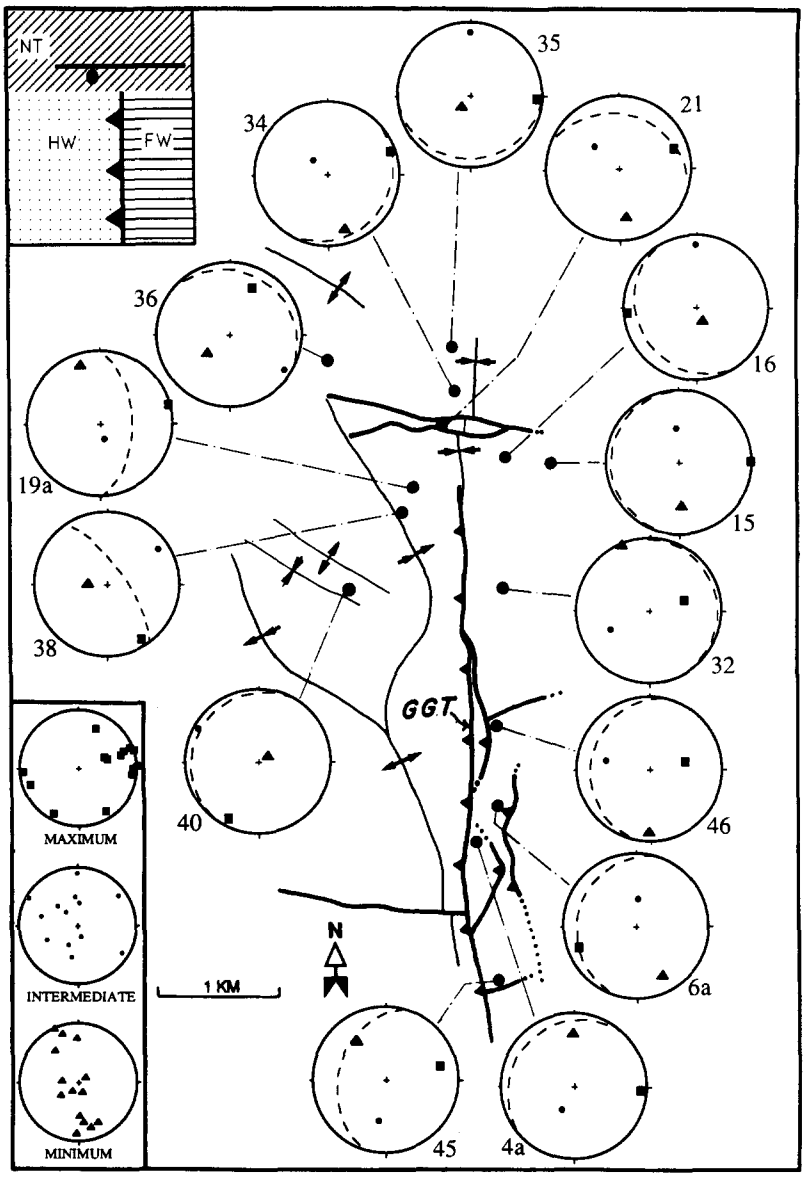

Fig. 8. Map showing sample locations and orientations of principal strain axes determined from calcite strain-gage measurements. Upper inset shows sample groupings as discussed in text. Lower inset shows composite stereonets of all principal strain data. Principal strain axes are shown on equal-area stereoplots: ε_1—squares, ε_2—dots and ε_3—triangles. Dashed great circles on stereoplots indicate bedding. GGT—Golden Gate thrust, NT—north of termination, HW—hangingwall, FW—footwall.

twin was assumed to be 0.5 times the measured thickness of the microtwin (Groshong 1974). After computing the best-fit strain tensor, each data set was 'cleaned' by two methods: (1) by removing the 20% of the measurements corresponding to the largest residuals; and (2) by removing all of the negative expected values (NEVs) from the original data set (Groshong *et al.* 1984). The best-fit strain tensor was then recalculated and the nominal errors of strain tensors computed from each cleaned data set were compared; the result with the lower nominal error from the two cleaning methods is reported in Table 1. The nominal error is computed from $0.5(\varepsilon_x + \varepsilon_y)$, where ε_x and ε_y are strain components normal to the x and y thin section co-ordinate system, respectively, and is considered to represent the goodness of fit of the inverted strain tensor to the data (Groshong 1972). In all but two samples (36 and 40), removing the 20% largest residuals resulted in substantially lower nominal errors. Samples 36 and 40 both had lower nominal errors when cleaned by removing NEVs, but the results were similar when cleaned by removing the 20% largest deviations.

Results of the calcite strain analysis are summarized in Table 1 and Fig. 8. In this study ε_1, ε_2 and ε_3 refer to maximum, intermediate and minimum principal shortening strains, respectively. Magnitudes of ε_1 are low, between -1.27 and -2.65%. This probably reflects the high fraction of microtwins in the samples. The ε_1 orientations trend E–W to ENE–WSW with shallow plunges, and in most cases are subparallel to bedding. The ε_3 orientations define a steeply dipping girdle that strikes NNW. ε_2 orientations show no clear preferred

Table 1. Calcite strain data

Sample No.	Sample location*	Magnitudes† ε_1 (%)	ε_2 (%)	ε_3 (%)	Error‖ (%)	Directions ε_1 T¶	ε_1 P¶	ε_2 T¶	ε_2 P¶	ε_3 T¶	ε_3 P¶	No. of NEVs/ No. of twins‡	S§ (%)
4A	FW	−1.73	0.11	1.6	0.24	95	11	206	60	359	27	7/41	0
6A	FW	−2.42	0.87	1.56	0.36	250	15	5	59	153	27	3/40	10
32	FW	−1.27	−0.43	1.70	0.19	69	48	246	42	337	1	0/40	40
45	FW	−2.36	0.23	2.13	0.22	73	25	191	45	324	34	3/42	100
46	FW	−1.88	−0.07	1.96	0.22	74	48	284	38	182	15	3/40	70
15	NT	−1.86	0.15	1.71	0.21	88	1	356	49	177	41	1/43	0
16	NT	−1.66	0.68	0.98	0.18	267	6	359	13	153	76	4/41	40
21	NT	−1.51	−0.08	1.59	0.2	69	19	315	51	172	33	2/43	50
34	NT	−1.58	0.60	0.98	0.16	69	9	319	66	163	23	4/41	100
35	NT	−2.41	0.82	1.59	0.09	92	9	0	12	217	75	2/47	50
36	NT	−2.65	0.61	2.04	0.16	25	28	122	13	234	59	2/37	100
19A	HW	−1.68	0.57	1.11	0.43	73	1	164	74	342	16	13/40	0
38	HW	−1.8	0.49	1.31	0.24	148	14	54	15	277	69	9/39	70
40	HW	−2.26	0.23	2.04	0.2	208	12	300	6	57	77	0/46	60

* Geographic location. NT means north of the thrust termination, FW means footwall, HW means hangingwall.
† Negative values are contractional.
‡ Number of negative expected values (NEVs)/number of twins after 'cleaning'.
§ Approximate percent of twins measured in sparry calcite to twins measured in fossil grains. A value of zero means all twins were measured in fossil grains.
‖ Error is the nominal error computed. See text.
¶ T = trend, P = plunge.

trend (Fig. 8). Most of the samples show significant departure from plane strain. Eleven of the 14 samples have a component of flattening.

The calcite strain data can be grouped according to their locations relative to the thrust tip. The locations are: (1) north of the thrust tip; (2) south of the thrust tip in the footwall; and (3) in the hangingwall (see inset, Fig. 8). These areas correspond roughly, but not precisely, to structural regions defined by bedding data (Fig. 6). Patterns of principal strain orientations within and between each group are discussed below.

Principal strains north of the thrust termination

In all samples collected north of the lateral termination, ε_1 orientations are sub-parallel to bedding. ε_1 orientations trend from 090° to 025° (Fig. 8). Sample 36 was collected from subhorizontal strata southwest of the Garden Valley anticline. The ε_1 orientation of 025° and steeply plunging ε_3 indicate that grain-scale plastic strains agree with map-scale deformation. The rest of the samples north of the termination were collected from near the northward projection or east of the Golden Gate thrust. They define ε_1 orientations that trend 44° or more clockwise relative to sample 36 (Fig. 8). This change within gently dipping, weakly faulted strata indicates significant variations in principal strain trajectories.

Five of the six samples collected in this region have moderate to steep ε_3 axes that plunge an average of 51°S (Fig. 8). If the samples record no volume change, then these data imply that the rocks were extended along a line that trends roughly N–S and plunges moderately to steeply south.

Principal strains in the footwall region

Samples collected from the footwall of the Golden Gate thrust have ε_1 orientations that trend E–W to ENE–WSW. Three of these samples define ε_1 orientations that are nearly parallel to bedding and two deviate as much as 45° from bedding.

The ε_1 orientations oblique to bedding suggest that footwall layer-parallel shear was accommodated by flexural flow within the layers rather than by flexural-slip between layers. This may account for the rareness of flexural-slip slickenlines in the footwall. The two samples with ε_1 orientations that are close to bedding-parallel (samples 4a and 6a) are from locations between imbricate thrusts (Fig. 8), where more of the strain may

Table 2. General outcrop descriptions of units that were sampled for the calcite strain-gage analysis

Unit	General description
Upper Joana Limestone	Thin- to medium-bedded, dark gray fossiliferous limestone. Local shale partings and chert stringers.
Lower Joana Limestone	Thick-bedded to massive, light to dark gray, coarsely-crystalline crinoidal limestone. Abundant bedding-parallel chert stringers.
Upper Guilmette Formation	Medium- to thick-bedded, dark bluish-gray limestone and dolomite. Locally fossiliferous.
Lower Guilmette Formation	Thin- to thick-bedded, light to dark gray limestone and dolomite. Locally fossiliferous.

have been accommodated by fault displacement and layer translation than by layer-parallel shear. Wiltschko *et al.* (1985), in contrast, found no deflection in ε_1 orientations but abundant interbed slip in beds moving over a thrust ramp. They interpreted this to mean that slip on bedding planes took place at less resolved shear stress than was required to twin calcite. The Golden Gate Range stratigraphic section appears to have a higher resistance to flexural-slip, perhaps a reflection of the predominance of relatively massive carbonate strata.

The ε_3 orientations for the footwall rocks generally trend approximately N–S and plunge an average of 21°, considerably shallower than those north of the thrust termination (Fig. 8). These data imply N–S extension in the footwall region in contrast to more vertical extension in the area north of the thrust termination.

Principal strains in the hangingwall region

Samples collected from the forelimb of the Golden Gate anticline define principal strain orientations that are quite different from samples elsewhere in the field area, especially those north of the thrust termination (Fig. 8). Sample 19a yielded an ε_1 orientation that is consistent with other samples but at a high angle to bedding, and sample 38 conforms neither with the rest of the data nor with map-scale structures. Forelimb rocks experienced strains that probably include layer-parallel shear as well as folding and thinning as the anticline formed. The more complex strain history inferred for these samples is corroborated by the large percentage of NEVs (Table 1), that is, twinned grains that record shear strains opposite in sense from that predicted from the best-fit strain tensor. In an attempt to separate distinct strain events, NEVs and PEVs (positive expected values) from these samples were analyzed separately (cf. Teufel 1980). However, this procedure still yielded large nominal errors (up to 0.74%; compare with Table 1) and no consistency between principal strain axis orientations between these forelimb samples. It appears that deformation in the forelimb was complex and inhomogeneous rather than recording overprinted strain events.

Sample 40 from the top of the Golden Gate anticline near the central folds and sample 36 from near the Garden Valley anticline yielded similar principal strain orientations (Fig. 8). The similarity of these data implies deformation in similar stress fields.

INTERPRETATION AND DISCUSSION

Lateral development of the thrust structures

Inspection of the sequence of cross-sections (Fig. 4) shows that it is impossible for the structure at the tip (section A–A′) to evolve into the structure far from the tip (section H–H′). For instance, the long forelimb in exposed Devonian rocks in section D–D′ should be preserved, if not lengthened, in sections farther to the south, yet this forelimb is nearly absent in southern sections. Further, geometrical models of fault-propagation folding predict fold-hinge migration (Suppe 1985). The upper flat top of a fault-propagation fold (line A–B′ in fig. 9-47 of Suppe 1985) shortens as the hinge migrates in the transport direction (B′ in fig. 9-47 of Suppe 1985). The analogous upper flat top of the Golden Gate anticline (the W-dipping limb, Fig. 4, sections F–F′ G–G′ and H–H′) appears to have remained stable; hinges that bound the upper flat do not migrate toward each other with increasing displacement. Thus the sequence of sections does not record the evolution of a growing fold from one section to the next.

The lateral termination of the Golden Gate thrust presently is located in a thrust-termination syncline. If the present thrust-termination structural geometries are typical of geometries when the thrust tip was farther south, then the synclinal portion of the footwall should be preserved there. The footwall south of section B–B′ is generally a W-dipping homocline (Fig. 6) and shows no evidence of a stranded footwall syncline.

Except for the two samples from the Golden Gate anticline forelimb, the calcite strain data indicate that, north of the termination, deformation in the footwall and on top of the Golden Gate anticline was relatively simple. The low number of NEVs suggest strain was coaxial and homogeneous throughout the period of deformation (Groshong 1974). In the ductile bead scenario, samples from locations south of the thrust termination would have been north of the termination at some point in the propagation history. They would have been subjected to stress orientations that changed as the fault-propagation fold approached and passed through the volume of rock (Pavlis & Bruhn 1988), and changes in response to hangingwall–footwall interactions with further displacement. Thus, those samples should record non-coaxial, inhomogeneous, and/or rotational strain which they do not appear to record.

Cross-section analysis, strain data and fold patterns from the southern Golden Gate Range contradict the predictions of a migrating ductile bead. The concentration of complex, three-dimensional structures near the final tip position suggest that the lateral termination of the Golden Gate thrust was already established as these structures grew in their present positions. We propose that the Golden Gate thrust propagated from the south to its present extent relatively quickly before much slip or hangingwall deformation had occurred. Julian & Wiltschko (1983) proposed this mechanism for the formation of the Sequatchie Valley anticline based on strain studies that indicated a simple strain history in the central part of the fold and complexity only at the lateral termination. Fischer & Woodward (1989, 1992) showed, based on geometrical analyses, that structures along the Rocky Valley thrust system in the Tennessee Valley and Ridge province and the Baldy thrust system in the Idaho–Wyoming thrust belt reflect effects of varying thrust trajectory and slip magnitude rather than recording passage of a ductile bead. They suggest that the structural variations primarily reflect variations in

intrinsic properties, such as thickness and unit competence of the rocks.

If the lateral tip of the Golden Gate thrust was locked in its present location during subsequent deformation, then it is reasonable to ask why propagation stopped at that location. Fischer & Woodward (1989, 1992) suggest that changes in the competence of rock units dictate the relative importance of faulting or folding (i.e. fault first or fold first) and that these changes can inhibit fault propagation in favor of folding. At a much smaller scale, Hyett (1990) interpreted the decrease in displacement of a small thrust in the Tutt Head thrust zone of South Wales to reflect resistance to faulting of relatively competent coarse grainstone. Julian & Wiltschko (1983) proposed that the position of the Sequatchie Valley anticline termination was predetermined by lateral facies changes. Morley (1987) attributed changes in deformation style and location of thrust tips to changes in rock competence in the Osen-Røa thrust sheet in Norway. However, in the southern Golden Gate Range, there are no significant lateral facies changes in the exposed section of rocks and no clear indications of why the Golden Gate thrust terminated where it did. At the present level of exposure, the Golden Gate thrust dies out in a 150+ m thick (top not preserved) section of Mississippian Chainman Shale (Fig. 3). The Chainman Shale is overlain by the Scotty Wash Quartzite (Tschanz & Pampeyan 1970) that crops out about 5 km north of the field area in the Golden Gate Range. The Scotty Wash Quartzite is the "least continuous Paleozoic unit in Lincoln County" and ranges in thickness from 0 to 800 m (Tschanz & Pampeyan 1970). We speculate that abrupt lateral changes in the thickness of the Scotty Wash Quartzite may have played an important role in the location of the Golden Gate thrust lateral termination.

We interpret the original fault to have propagated with little slip to near its present extent. Cross-cutting relationships between fault X and the eastern and western thrust splays, as well as hangingwall–footwall relations across the east splay, indicate that the eastern splay was the original fault surface. As displacement and deformation ensued, the thrust broke through the highly fractured and weakened forelimb after the eastern splay accumulated about 375 m displacement at section E–E′ (Fig. 4). Thus, the western splay is interpreted as a back-breaking thrust that formed later in the displacement history, caused the abandonment of the eastern splay, and stranded the vertical section of rocks between the splays.

The interpretation that structures around the thrust tip grew while it was pinned at its present location does not preclude the possibility that the Golden Gate thrust previously was temporarily pinned elsewhere farther south. Comparison of macroscopic and microscopic strain features preserved farther south along the thrust compared to that preserved near the thrust tip suggest that such temporary pinning occurred. These features include the following. (1) The orientations and geographic locations of the central folds on top of the Golden Gate anticline relative to the thrust trace and strike are very similar to those of the Garden Valley anticline (Fig. 2). It is difficult to determine unequivocally the relative timing of the Golden Gate anticline, Garden Valley anticline and central folds; it is possible that the Garden Valley anticline and central folds formed later in a stress regime different from that during thrust deformation. However, the simple calcite strain data for samples in both areas (Table 1) suggest that deformation did not occur in multiple stress regimes. (2) Calcite strain data from near the central folds yield almost the same principal strain orientations as the sample collected the same distance west of the thrust or its projected strike (compare samples 36 and 40, Fig. 8). (3) Fault X has a similar orientation, sense of offset and north-to-south bedding discordance as the North Canyon faults. (4) The decrease in lateral displacement gradient between sections C–C′ and D–D′ and the increase between sections D–D′ and E–E′ (Fig. 7) may be due to the thrust tip being temporarily pinned near section D–D′. This hypothesis is corroborated by the observation that the central folds and fault X are located relative to this possible temporary tip location much as the Garden Valley anticline and North Canyon faults are located relative to the final tip location. This location further suggests that splaying of the thrust in this area may be related to propagation of the fault past the locked tip.

Structural evidence from the southern Golden Gate Range suggests that thrust-related folds did not form in a migrating ductile bead. The thrust quickly propagated along strike to its present length, i.e. faulting occurred before folding. Variations in deformation along strike were determined by location with respect to a fixed lateral terminus.

Deformation at the lateral tip

The Garden Valley anticline and calcite strain data record NNE–SSW contraction northwest of the thrust tip, and the North Canyon faults and calcite strain data record N–S extension at the tip and in the footwall. Although there is no evidence of a physical shear plane, the eastward transport of the Golden Gate thrust hangingwall rocks relative to the rocks north of the termination suggests an E–W vertical shear system north of the termination. Several observations suggest that deformation northwest of the lateral tip cannot be explained by a simple shear mechanism alone, but may be better explained by transpression, which is the coupling of simple shear with a component of shortening normal to the shear boundary (Harland 1971, Sanderson & Marchini 1984, Sylvester 1989). First, the calcite strain data (Table 1) show that there is a significant flattening component in five of the six samples north of the thrust termination; simple shear requires a plane strain condition. Second, if the strains were due only to simple shear along a vertical plane, one would expect the ε_3 axes from the calcite strain analysis to be horizontal rather than steeply plunging. Third, the trend of the Garden Valley anticline and the ε_3 orientation from

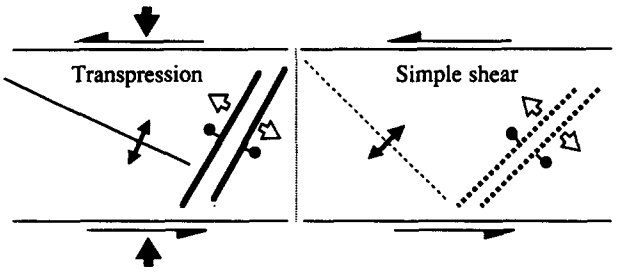

Fig. 9. Diagram showing fold and normal-fault orientations in a sinistral transpression zone. Arrows on normal faults show relative extension direction in the transpression zone. Folds and faults of similar orientations are located near the Golden Gate thrust termination (cf. Figs. 2 and 6).

sample 36 (Fig. 8) are more westerly than predicted for an échelon folding by simple shear. Fourth, the NE strike of the normal faults north of the North Canyon faults is similar to that predicted for transpression. As is shown in Fig. 9, folds trend at a smaller angle to the shear direction than predicted for simple shear and normal faults form at a higher angle to the shear direction.

The shear strain at the lateral tip can be estimated by considering the amount of shear between slipped and laterally equivalent unslipped regions of the thrust and by assuming that the displacement gradient remains constant along blind sections of thrust north of its termination. For the Golden Gate thrust, 2.4 km of slip variation in 7 km of strike length results in a shear strain of 0.36. However, this value is from shear in a plane parallel to the Golden Gate thrust; in the transpression model shear is swept out in a horizontal plane. Assuming the thrust ramp angle is 45°, the horizontal component of the shear strain is 0.24. Sanderson & Marchini (1984) show that transpression requires a vertical ε_3 or ε_2 orientation. The subvertical plane containing ε_3 and ε_2 defines an angle θ' to the shear boundary which can be used with the shear strain to estimate the relative shortening and stretching across the transpression zone (fig. 2 of Sanderson & Marchini 1984). Using a shear strain of 0.24 and $\theta' = 30°$, the stretch normal to the shear zone (N–S) is about 0.9, i.e. about 10% N–S shortening is predicted in the vicinity of the Garden Valley anticline. A N–S cross-section across the Garden Valley anticline indicates that it accommodates about 7% shortening, but additional shortening is probably accommodated by calcite strain and by pressure solution.

The North Canyon faults are interpreted to be related to differential uplift and the resistance to folding of rocks north of these faults. A hypothesis for the formation of the transpression and extensional zones is illustrated in Fig. 10. As slip accumulates, the anticline–syncline pair forms at the thrust tip and point A is uplifted higher than stratigraphically equivalent point B. Bending stresses caused by differential fault slip and uplift of the anticline result in a reoriented maximum compressive stress at the lateral tip of the fold (σ_1 orientation in Fig. 10b). Pavlis & Bruhn (1988) calculated a rotation of up to 30° in σ_1 orientation at a lateral termination fold. Julian & Wiltschko (1983) also reported 20–30° stress reorien-

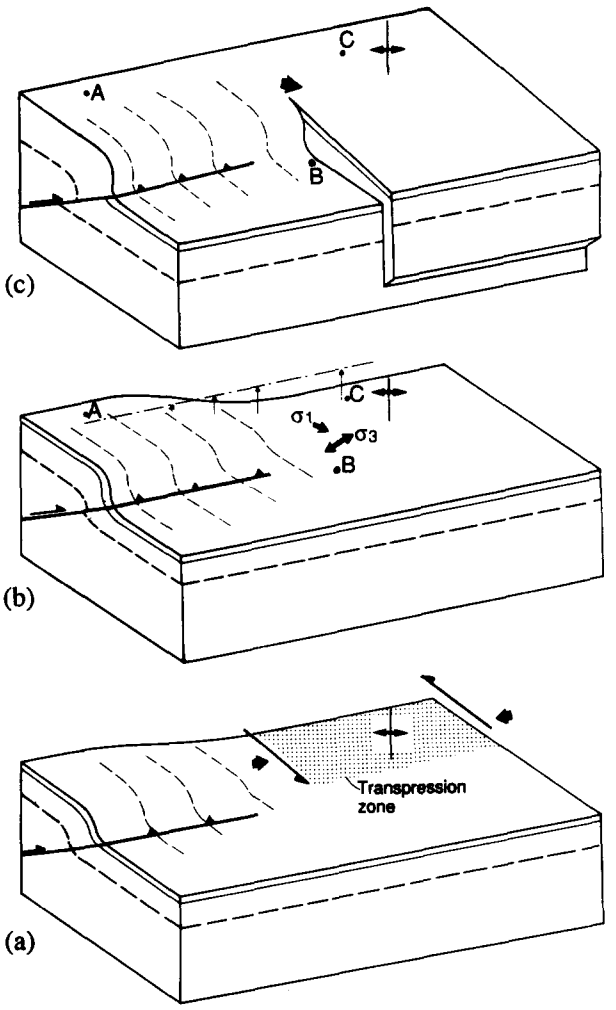

Fig. 10. Block diagrams showing interpretation of the development of structures at the lateral tip of the Golden Gate thrust. (a) Area north of the lateral tip develops NW-trending folds in the inferred transpression zone. Large arrows outside the transpression zone show shear sense. (b) Continued displacement on the Golden Gate thrust with a pinned lateral tip. σ_1 and σ_3 arrows show inferred local orientations of maximum and minimum principal stresses, respectively. Vertical arrows show eventual uplift direction of rocks farther north. (c) Present geometry of the Golden Gate thrust and related structures. See discussions in text.

tations based on Turner compression axes and dominant joint sets at the termination of the Sequatchie Valley thrust anticline. The North Canyon faults are interpreted to have formed by extension as point C, part of a structurally coherent block attached to the crest of the hangingwall anticline, was tilted and translated northeast relative to point B. Thus the North Canyon faults separate rigid-block tilting and northeast translation on the north from folding on the south, and probably reflect the resistance of brittle rocks to folding. Had the thrust propagated farther north from its present terminus, it would have stranded the eastern part of North Canyon faults in the thrust footwall and western part in the thrust hangingwall.

At first glance the North Canyon faults appear to be simple tear faults that transfer displacement between two thrust segments. However, the Golden Gate thrust dies out south of the North Canyon faults at the

erosional surface (Fig. 2). The North Canyon faults therefore do not transfer displacement between thrust segments, but rather accommodate the abrupt termination of the Golden Gate anticline–syncline pair at the thrust terminus.

It is unknown why the North Canyon faults are located where they are. Their location might depend on pre-existing zones of weakness or depend on competency and thickness changes of rocks up-section that have been removed by erosion. N–S extension may have been initiated in response to initial formation of the thrust-termination syncline. This extension (recorded by calcite strain data), along with counterclockwise rotation of σ_1 northwest of the thrust tip, may have resulted in an extensional zone in the synclinal area of the tip. This zone could later have acted as a zone of weakness that allowed the North Canyon faults to form during subsequent hangingwall uplift.

The North Canyon faults have possible neotectonic implications. During an earthquake, point A in Fig. 10 is uplifted a discrete amount relative to points B and C. The vertical arrows on Fig. 10(b) show the later uplift during stress relaxation that would occur as points north of A incrementally attempt to 'catch-up' to A. In this manner point C is uplifted relative to stationary point B and the lateral-termination extensional faults form between. Philip & Meghraoui (1983) mapped small tensile surface breaks at the terminations of thrust surface rupture segments from the El Asnam earthquake, indicating that earthquake-related oblique extensional features do occur at lateral terminations of active thrust faults.

CONCLUSIONS

Displacement across the Golden Gate thrust increases southward from zero at the exposed northern lateral tip to a maximum of 2.4 km about 5 km along strike (two-thirds of the exposed strike length) with an average lateral displacement gradient of 0.42. The southern 2 km of exposed strike length defines a constant displacement of 2.4 km.

Major folding associated with thrusting includes two types. First, a hangingwall anticline, the Golden Gate anticline, is cylindrical where it trends parallel to the thrust and thrust displacement is constant. Farther north where thrust displacement decreases, this anticline bifurcates and bends into a steep-limbed box fold that is oriented about 20° counterclockwise relative to the thrust strike. Second, an anticline that trends 25° relative to the hangingwall anticline is located northwest of the thrust tip. Comparably oriented folds also appear on the flat crest of the box fold part of the Golden Gate anticline.

Faulting near the termination that is associated with thrust displacement includes: (1) E–W-striking normal faults (the North Canyon faults) that record extension at the lateral tip; (2) NE-striking normal faults north of the thrust slip; (3) shallowly-dipping footwall imbricates with minor displacement; and (4) a backward-breaking splay that became the main slip surface and steepened the thrust.

We interpret the structures at the lateral tip to have formed while the tip was locked at its present position rather than by a fold-first ductile bead process. This interpretation is dictated by: (1) the lack of a record of progressive evolution between sequential cross-sections along strike; (2) the lack of evidence for progressive fold-hinge migration along the trend of the hangingwall anticline; and (3) calcite strain data that do not record anticipated inhomogeneous, non-coaxial progressive deformation. Thus, the Golden Gate thrust probably propagated to the north relatively quickly with little displacement, indicating it was easier to fault the rocks than to fold them. Calcite strain data and a lack of flexural-slip striae in the thrust footwall also suggest that resistance to flexural-slip, and therefore to buckle folding, was relatively high. The presence of structures to the south of the ultimate tip location that are similar to those found at the thrust tip suggest that the lateral tip may have been temporarily locked about 2 km south of the ultimate terminus, and that splaying of the thrust in that area may be related to the process of breaking through the locked tip.

Structural, kinematic and strain data suggest deformation north of the lateral tip is consistent with transpression and later uplift. During transpression, the rocks north of the lateral tip would have been subjected to sinistral shear possibly along an E–W-striking vertical plane and a component of N–S shortening across the shear zone. N–S extension at the lateral tip was caused by uplift and northeast translation of the thrust hangingwall together with rocks north of the North Canyon faults, relative to the synclinal rocks to the south. Extension resulted in the formation of the North Canyon faults.

Acknowledgements—This study was partially funded by research grants from Sigma Xi, the Geological Society of America, the American Association of Petroleum Geologists, Mobil Exploration & Producing, U.S., Inc., Marathon Oil Company, and two University of Utah Graduate Research Fellowships to P. Armstrong. We thank Jim Evans, John O. D. Byrd and John Fletcher for reviewing early versions of the manuscript and making helpful suggestions. Jim Evans, Paul Genovese and Mark Evans provided help and useful suggestions on the calcite strain-gage technique. Richard Groshong provided the code from his original version of the strain-gage program. Discussions of the structures with Ron Bruhn and Wanda Taylor were very helpful and Patricia Butcher was an extremely valuable field assistant. The stereonet program written by R. Allmendinger was used to plot structural and strain data. Critical reviews by S. Wojtal, an anonymous referee, and especially D. Wiltschko and N. Woodward provided insight that helped us substantially change our interpretations for the better.

REFERENCES

Armstrong, R. L. 1968. Sevier orogenic belt in Nevada and Utah. *Bull. geol. Soc. Am.* **79**, 429–458.

Boyer, S. E. & Elliott, D. 1982. Thrust systems. *Bull. Am. Ass. Petrol. Geol.* **66**, 1196–1230.

Chapman, T. J. & Williams, G. D. 1984. Displacement–distance methods in the analysis of fold–thrust structures and linked-fault systems. *J. geol. Soc. Lond.* **141**, 121–128.

Chapman, T. J. & Williams, G. D. 1985. Strains developed in the hanging walls of thrusts due to their slip/propagation rate: a dislocation model: reply. *J. Struct. Geol.* **7**, 759–762.
Chester, J. S. & Chester, F. M. 1990. Fault-propagation folds above thrusts with constant dip. *J. Struct. Geol.* **12**, 903–910.
Dahlstrom, C. D. A. 1969. Balanced cross sections. *Can. J. Earth Sci.* **6**, 743–757.
De Paor, D. G. 1988. Balanced section in thrust belts part 1: construction. *Bull. Am. Ass. Petrol. Geol.* **72**, 73–90.
Elliott, D. 1976. The energy balance and deformation mechanisms of thrust sheets. *Phil. Trans. R. Soc. Lond.* **283**, 289–312.
Evans, J. P. & Spang, J. H. 1984. The northern termination of the Crawford thrust, western Wyoming. *Contr. Geol. Univ. Wyoming* **23**, 15–31.
Fischer, M. P. & Woodward, N. B. 1989. Non-eulerian systems in Tennessee and Wyoming. *Geol. Soc. Am. Prog. w. Abs.* **21**, 135.
Fischer, M. P. & Woodward, N. B. 1992. The geometric evolution of foreland thrust systems. In: *Thrust Tectonics* (edited by McClay, K. L.). Chapman & Hall, London, 181–189.
Geiser, P. A. 1988. The role of kinematics in the construction and analysis of geological cross sections in deformed terranes. In: *Geometries and Mechanics of Thrusting with Special Reference to the Appalachians* (edited by Mitra, G. & Wojtal, S.). *Spec. Pap. geol. Soc. Am.* **222**, 47–76.
Groshong, R. H., Jr. 1972. Strain calculated from twinning in calcite. *Bull. geol. Soc. Am.* **83**, 2025–2038.
Groshong, R. H., Jr. 1974. Experimental test of least-squares strain-gage calculation using twinned calcite. *Bull. geol. Soc. Am.* **85**, 1855–1864.
Groshong, R. H., Jr., Teufel, L. W. & Gasteiger, C. 1984. Precision and accuracy of the calcite strain-gage technique. *Bull. geol. Soc. Am.* **95**, 357–363.
Harland, W. B. 1971. Tectonic transpression in Caledonian Spitsbergen. *Geol. Mag.* **108**, 27–42.
Heim, A. 1921. *Geologie der Schweiz, II. Die Schweizer Alpen.* Tauchnitz, Leipzig.
Heller, P. L. & Paola, C. 1989. The paradox of Lower Cretaceous gravels and the initiation of thrusting in the Sevier orogenic belt, United States Western Interior. *Bull. geol. Soc. Am.* **101**, 864–875.
Hertzberg, R. W. 1976. *Deformation and Fracture Mechanics of Engineering Materials.* Wiley, New York.
Hyett, A. J. 1990. Deformation around a thrust tip in Carboniferous limestone at Tutt Head, Near Swansea, South Wales. *J. Struct. Geol.* **12**, 46–58.
Jamison, W. R. 1987. Geometric analysis of fold development in overthrust terranes. *J. Struct. Geol.* **9**, 207–219.
Julian, F. E. & Wiltschko, D. V. 1983. Deformation mechanisms in a terminating thrust anticline, Sequatchie Valley, Tennessee. *Geol. Soc. Am. Prog. w. Abs.* **15**, 606.
Morley, C. K. 1987. Lateral and vertical changes of deformation style in the Osen-Røa thrust sheet, Oslo region. *J. Struct. Geol.* **9**, 331–343.
Pavlis, T. L. & Bruhn, R. L. 1988. Stress history during propagation of a lateral fold-tip and implications for the mechanics of fold-thrust belts. *Tectonophysics* **145**, 113–127.
Phillip, H. & Meghraoui, M. 1983. Structural analysis and interpretation of the surface deformations of the El Asnam earthquake of October 10, 1980. *Tectonics* **2**, 17–49.
Reso, A. 1963. Composite columnar section of exposed Paleozoic and Cenozoic rocks in the Pahranagat Range, Lincoln County, Nevada. *Bull. geol. Soc. Am.* **74**, 901–918.
Rowan, M. G. & Ratliff, R. A. 1988. Use of fault cut-offs and bed travel distance in balanced cross-sections: Discussion 1. *J. Struct. Geol.* **10**, 311–316.
Sanderson, D. J. & Marchini, W. R. D. 1984. Transpression. *J. Struct. Geol.* **6**, 449–458.
Snyder, D. B. 1983. Interpretation of the Bouguer gravity map of Nevada. *Nev. Bur. Mines Geol. Rep.* 37.
Spang, J. H. & Van Der Lee, J. 1975. Numerical dynamic analysis of quartz deformation lamellae and calcite and dolomite twin lamellae. *Bull. geol. Soc. Am.* **86**, 1266–1272.
Suppe, J. 1983. Geometry and kinematics of fault-bend folding. *Am. J. Sci.* **283**, 684–721.
Suppe, J. 1985. *Principles of Structural Geology.* Prentice-Hall, Englewood Cliffs, New Jersey.
Sylvester, A. G. 1989. Strike-slip faults. *Bull. geol. Soc. Am.* **100**, 1666–1703.
Teufel, L. W. 1980. Strain analysis of experimental superposed deformation using calcite twin lamellae. *Tectonophysics* **65**, 291–309.
Tschanz, C. M. & Pampeyan, E. H. 1970. Geology and mineral deposits of Lincoln County, Nevada. *Nev. Bur. Mines Geol. Bull.* **73**.
Williams, G. D. & Chapman, T. J. 1983. Strains developed in the hanging wall of thrusts due to their slip/propagation rate; a dislocation model. *J. Struct. Geol.* **5**, 567–571.
Wiltschko, D. V., Medwedeff, D. A. & Millson, H. E. 1985. Distribution and mechanisms of strain within rocks on the northwest ramp of Pine Mountain block, southern Appalachian foreland: A field test of theory. *Bull. geol. Soc. Am.* **96**, 426–435.
Woodward, N. B., Boyer, S. E. & Suppe, J. 1985. An Outline of Balanced Sections (2nd edn). *Knoxville Univ. Tennessee, Dept Geol. Sci., Stud. Geol.* **11**.

APPENDIX
DISPLACEMENT UNCERTAINTIES

The major sources of displacement uncertainty, assuming the Golden Gate thrust is planar, arise from projecting the footwall and hangingwall contacts into the Golden Gate thrust. Figure A1 shows the geometric relationships used to estimate uncertainties in location of hangingwall and footwall cutoffs. In the footwall, the cutoff uncertainty estimates were made by allowing the contact dips to vary ±5°. This probably is reasonable in light of Coal Valley dip-meter data in which most of the dips lie within 5° of the mean dip for the entire Paleozoic section penetrated by the well. The pivot point of the 5° variation is at the intersection of the contact and a line (hinge line in Fig. A1) that is perpendicular to bedding and intersects the ground surface near the Golden Gate thrust (Fig. A1).

In the hangingwall, the largest cutoff uncertainty is assumed to result from forelimb thinning. Forelimb thinning varies between 0 and 40%, and averages about 20%, as drawn in the cross-sections. The best constrained contact (cut-off closest to the surface) for each cross-section was picked as a datum contact from which all the thickness changes were measured in a cross-section. The uncertainty in locating

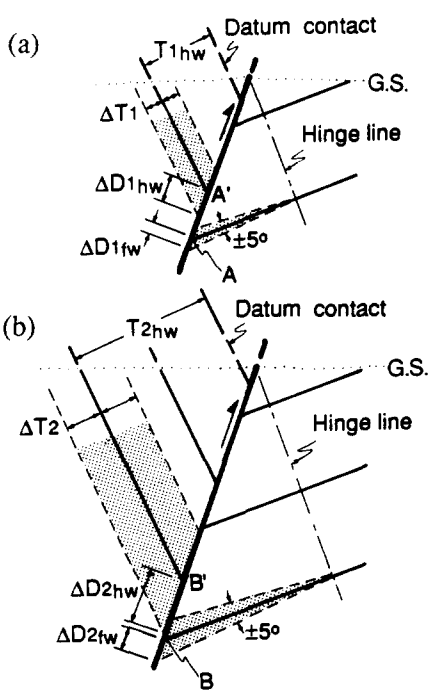

Fig. A1. Schematic diagram showing geometrical relationships used to quantify displacement uncertainties for (a) a shallow contact and (b) a second, deeper contact. The stippled regions illustrate uncertainties as discussed in text. Note that the stippled regions are larger for contacts farther from the datum contact in the hangingwall and from the ground surface (G.S.) in the footwall. $\Delta D1_{hw}$, $\Delta D2_{hw}$ and $\Delta D1_{fw}$, $\Delta D2_{fw}$ refer to uncertainties in cutoff positions in the hangingwall and footwall, respectively, for displacements between points A–A′ and B–B′ (A–A′ < B–B′). $T1_{hw}$ and $T2_{hw}$ are forelimb units that are 20% thinner than their footwall counterparts.

Table A1. Displacements and estimated uncertainties in m

Contact	A–A'*	B–B'†	C–C'	D–D'	E–E'‡	F–F'§	G–G'§	H–H'§
M–Dg	30	305 + 90	700 + 215	790 + 245	855 + 760	2135 + 425	2285 + 425	2255 + 455
		− 90	− 215	− 245	− 215	− 425	− 425	− 455
Dg–Dsi	150	395 + 210	825 + 90	945 + 180	1465 + 185	2165 + 365	2345 + 305	2320 + 365
		− 180	− 90	− 180	− 185	− 365	− 305	− 365
Dsi–Dse	215	455 + 365	975 + 215	1005 + 215	1645 + 185	2345 + 275	2440 + 245	2385 + 355
		− 245	− 215	− 215	− 185	− 275	− 245	− 335
Dse–SOu	245	550 + 425	1065 + 335	1100 + 305	1735 + 275	2440 + 245	2440 + 245	2440 + 275
		− 335	− 335	− 305	− 275	− 245	− 245	− 275
SOu–Op	335	610 + 580	1160 + 455	1160 + 455	1800 + 490	2440 + 365	2470 + 335	2470 +245
		− 400	− 455	− 455	− 490	− 365	− 335	− 245
Op–Cu	500	1070 + 915	1250 + 730	1220 + 640	2075 + 640	2590 + 700	2745 + 520	2745 + 455
		− 730	− 730	− 640	− 640	− 700	− 520	− 455

* Estimated from projection of contacts into plane of section B–B'. See text.
† Positive and negative uncertainties differ because of assumption that displacement decreases toward frontal tip.
‡ Large positive error for M–Dg contact is due to uncertainty in projecting vertical contacts between splays.
§ Includes an estimated ± 120 m uncertainty across footwall splays for M–Dg contact.

hangingwall cutoffs ($\Delta D1_{hw}$ and $\Delta D2_{hw}$ in Fig. A1) of contacts above or below the datum were measured directly from the cross sections by varying the location of the contacts ±20% of their original (pre-thinned) thickness (ΔT1 and ΔT2 in Fig. A1). Uncertainties in the hangingwall cutoff location for contacts that project into the air were handled in exactly the same fashion, and thicknesses were measured from the same datum contact. Uncertainties caused by varying the forelimb thicknesses are large compared to varying the forelimb dip by small amounts, and therefore forelimb dip variations were neglected.

The hangingwall and footwall cutoff uncertainties were summed to give the total uncertainty for any contact. Additional cutoff location uncertainties arise because of splaying and imbrication of the Golden Gate thrust. These were added to the total hangingwall–footwall uncertainties and are noted in Table A1. In both the hangingwall and footwall, the geometric properties of this analysis produce small cutoff uncertainties for well-constrained contacts close to the surface and larger uncertainties for deeper contacts. This is illustrated in Fig. A1 by the larger stippled areas for deep contacts. Thus cutoff uncertainties accumulate with depth or with projection into the air. Because the contacts do not intersect the fault at 90°, cutoff uncertainties related to positive vs negative dip and thickness variations have different magnitudes, and therefore the larger uncertainty was chosen.